The Journal of Immunology

T Cell-Dendritic Cell Immunological Synapses Contain TCR-dependent CD28-CD80 Clusters That Recruit Protein Kinase C θ

Su-Yi Tseng, Janelle C. Waite, Mengling Liu, Santosha Vardhana and Michael L. Dustin

J Immunol 2008; 181:4852-4863; ;
doi: 10.4049/jimmunol.181.7.4852
http://www.jimmunol.org/content/181/7/4852

The Journal of Immunology is published twice each month by
The American Association of Immunologists, Inc.,
1451 Rockville Pike, Suite 650, Rockville, MD 20852

Print ISSN: 0022-1767 Online ISSN: 1550-6606.

T Cell-Dendritic Cell Immunological Synapses Contain TCR-dependent CD28-CD80 Clusters That Recruit Protein Kinase Cθ[1]

Su-Yi Tseng,[2]* Janelle C. Waite,* Mengling Liu,† Santosha Vardhana,* and Michael L. Dustin[3]*

Short-lived TCR microclusters and a longer-lived protein kinase Cθ-focusing central supramolecular activation cluster (cSMAC) have been defined in model immunological synapses (IS). In different model systems, CD28-mediated costimulatory interactions have been detected in microclusters, the cSMAC, or segregated from the TCR forming multiple distinct foci. The relationship between TCR and costimulatory molecules in the physiological IS of T cell-dendritic cell (DC) is obscure. To study the dynamic relationship of CD28-CD80 and TCR interactions in the T cell-DC IS during Ag-specific T cell activation, we generated CD80-eCFP mice using bacterial artificial chromosome transgenic technology. In splenic DCs, endogenous CD80 and CD80-eCFP localized to plasma membrane and Golgi apparatus, and CD80-eCFP was functional in vivo. In the OT-II T cell-DC IS, multiple segregated TCR, CD80, and LFA-1 clusters were detected. In the T cell-DC synapse CD80 clusters were colocalized with CD28 and PKCθ, a characteristic of the cSMAC. Acute blockade of TCR signaling with anti-MHC Ab resulted in a rapid reduction in Ca^{2+} signaling and the number and size of the CD80 clusters, a characteristic of TCR microclusters. Thus, the T cell-DC interface contains dynamic costimulatory foci that share characteristics of microclusters and cSMACs. ***The Journal of Immunology,*** **2008, 181: 4852–4863.**

Primary helper T cell activation requires the presentation of MHC class II-antigenic peptide complexes (MHCp)[4] and costimulatory ligands by dendritic cells (DC). These interactions induce T cell deceleration and formation of stable T cell-DC synapses (1–5). Most of what we know about the molecular details of the stable immunological synapse (IS) comes from the study of simplified model systems that replace the DC with a transformed non-DC cell type or supported planar bilayer (6–12).

Model ISs are characterized by formation of radially symmetric multimicrometer scale supramolecular activation clusters (SMACs). When MHCp density is high, the bulk of the TCR can be located in the central SMAC (cSMAC), which is also enriched in protein kinase Cθ (PKCθ) (7, 9). The amount of TCR accumulated in the cSMAC is proportional to the density of MHCp presented (13). The cSMAC is surrounded by a symmetrical peripheral SMAC (pSMAC) enriched in LFA-1 and talin (9) and a distal SMAC enriched in F-actin and CD45 (14, 15). Although this organization was observed with mature DC in one study, others have found that T cell-DC interfaces have multiple large TCR clusters rather than a single cSMAC (16, 17).

Before SMAC formation, TCR are engaged in the periphery of the nascent IS (7) in microclusters (10). After SMACs are established, the ongoing formation of TCR microclusters is required for sustained signaling when T cells are activated by planar bilayers (13, 18, 19), but this remains to be clearly demonstrated with cells presenting MHCp. Microclusters are dynamic and have a lifetime of ~2 min, the time required for their disappearance after addition of anti-MHCp Abs that block new TCR-MHCp interactions (13). The cSMAC is relatively more stable than microclusters in that it persists for >20 min after anti-MHCp Abs (13). In summary, TCR are engaged in two structures, short-lived microclusters linked to sustain TCR signaling and a relatively long-lived cSMAC that focuses on PKCθ.

The key costimulatory receptor CD28 has also been studied primarily in model systems and not previously with DC. Presentation of CD80 along with MHCp on B cell tumors enhanced IS formation (20). CD28-CD80 interactions accumulate in the cSMAC in a TCR-dependent manner (21, 22). Before cSMAC formation, CD28 accumulates in TCR microclusters (23). This suggests that the CD28 focused in the cSMAC is recruited via the TCR microclusters and this may account for the TCR dependence. The recruitment of PKCθ to the cSMAC is dependent upon CD28-CD80 interactions and specific sequences in the cytoplasmic domain of CD28 (11). We have previously observed using a model system

*Program in Molecular Pathogenesis, Helen L. and Martin S. Kimmel Center for Biology and Medicine of the Skirball Institute of Biomolecular Medicine and Department of Pathology, New York University School of Medicine, New York, NY 10016; and †Division of Biostatistics, New York University Cancer Institute, New York, NY 10016

Received for publication February 25, 2008. Accepted for publication July 23, 2008.

The costs of publication of this article were defrayed in part by the payment of page charges. This article must therefore be hereby marked *advertisement* in accordance with 18 U.S.C. Section 1734 solely to indicate this fact.

[1] This work was supported by National Institutes of Health Grants AI55037, AI43542, and AI44931 (to M.L.D.). S.-Y.T. was a recipient of Leukemia and Lymphoma Society Fellowship Grant 5456-04. M.L.D. was supported by National Cancer Institute Cancer Center Support Grant P30 CA016087.

[2] Current address: Geron Corporation, 230 Constitution Drive, Menlo Park, CA 94025.

[3] Address correspondence and reprint requests to Dr. Michael L. Dustin, Helen L. and Martin S. Kimmel Center for Biology and Medicine of the Skirball Institute of Biomolecular Medicine, New York University School of Medicine, 540 First Avenue, New York, NY 10016. Email address: dustin@saturn.med.nyu.edu

[4] Abbreviations used in this paper: MHCp, MHC class II-antigenic peptide complex; eCFP, enhanced cyan fluorescence protein; IS, immunological synapse; DC, dendritic cell; SMAC, supramolecular activation cluster; cSMAC, central SMAC; PKCθ, protein kinase Cθ; pSMAC, peripheral SMAC; BAC, bacterial artificial chromosome; Tg, transgenic; CHO, Chinese hamster ovary; 3D, three dimensional; qvtr, quick-time virtual reality; WT, wild type; MTOC, microtubule-organizing center; Treg, regulatory T cell.

that the cytoplasmic domain of CD80 controls the multimicrometer scale segregation of TCR clusters from CD28-CD80 clusters (12). This model also revealed that when CD28-CD80 clusters are segregated from TCR clusters, the PKCθ is focused in the CD28-CD80 clusters (12). In summary, CD28-CD80 clusters can be segregated from TCR clusters in model systems, but the dynamics of these structures are not known in any system and costimulation has not been studied at all in critically important T cell-DC IS.

In this study, we examined the dynamics of CD80, TCR, and LFA-1 accumulation in the T cell-DC IS and tested the ongoing requirement for new TCR-MHCp interactions in sustaining CD80, TCR, and LFA-1 clusters. Using DC from CD80-enhanced cyan fluorescence protein (eCFP) bacterial artificial chromosome (BAC)-transgenic (Tg) mice and immunofluorescence microscopy, we were able to monitor CD80 clustering longitudinally with live conjugates without modification of CD28 on the T cells. This approach allowed us to analyze the dependence of CD80 clustering in the IS with respect to dynamic TCR interactions that were controlled temporally using anti-MHC Abs. In T cell-DC IS, we observed multiple clusters containing CD80, TCR, or LFA-1, but not in combination. CD80 clusters uniquely focused PKCθ. Inhibition of new TCR-MHCp interactions with anti-I-A^b, MHC-blocking Ab, rapidly reduced Ca^{2+} signaling to baseline and abrogated CD80 clustering, reduced TCR clustering, but did not alter LFA-1 clustering in 4–5 min. This suggests that CD80 clusters share properties of microclusters (short lifetime after TCR blocking) and the cSMAC (focusing of PKCθ in stable IS).

Materials and Methods

Mice and peptides

The vector containing *CD80-eCFP* used to generate BAC Tg mice were constructed by inserting eCFP (BD Clontech) to the end of the *CD80* cytoplasmic tail of BAC clone RP23-69GS (National Center for Biotechnology Information). The linker sequence used and the BAC Tg construct generation method has been described elsewhere (12, 24). In brief, PCR-positive RP23-69GS clone was grown to log phase, pelleted, and washed three times with 10% glycerol while keeping everything at 4°C. H5.3 shuttle vector (1 μg/μl) containing 1 kb of *CD80* sequences flanking both sides of *eCFP* was added to 50 μl of the resuspended cells and electroporated at 1800 Ω and 2.5 W. After shaking for 30 min in 1 ml of Super Optimal Broth medium, 900 μl of the cell pellet was added to plates containing 12.5 μg/ml chloramphenicol and 30 μg/ml ampicillin. Colonies positive for integration were identified by PCR and streaked on sucrose plates to grow for 3 days at 37°C. Positive colonies for resolution were first identified by PCR and by pulse-field gel electrophoresis and confirmed by Southern blot. Purified BAC DNA was injected into F2 B6 blastocytes by the staff of the University of Michigan transgenic core facility. Positive founders were screened by PCR with 5′-CACTATGCTATGAGA-3′ and 5′-GGAC ACGCTGAACTTGTG-3′. Expression of CD80-eCFP was confirmed by immunofluorescence microscopy.

The F2 C57BL/6 founders were crossed to CD80/CD86$^{-/-}$ on the C57BL/6 background purchased from The Jackson Laboratory. OT-II C57BL/6 (H-2^b) CD4$^+$ TCR Tg mice purchased from The Jackson Laboratory were crossed to C57BL/6 Rag2$^{-/-}$ mice. B10.A 5C.C7 TCR (Vα11Vβ3) Tg mice were purchased from Taconic Farms. All mice were maintained under specific pathogen-free conditions at the Skirball Institute animal care facility at New York University in accordance with the Institutional Animal Care and Use Committee guidelines. MCC_{88-103} (AN ERADLIAYLKQTK) and $OVA_{323-339}$ (ISQAVHAAHAEINEAGR) were synthesized by the Dana-Farber Cancer Institute peptide synthesis facility (Boston, MA).

Immunoprecipitation and Western blot

LPS/anti-CD40- treated and untreated CD11c$^+$ splenocytes were lysed using an immunoprecipitation kit with protein A (Roche Applied Science) according to the manufacture's protocol. The target samples were immunoprecipitated overnight at 4°C with rabbit polyclonal anti-GFP Ab (Sigma-Aldrich). The immunoprecipitated protein samples were reduced with 2-ME and separated by 10% SDS-PAGE (Bio-Rad) with Kaleidioscope Prestained Standards (Bio-Rad), than transferred to polyvinylidene difluoride membranes (Bio-Rad) at 4°C for 4 h. The sample was immunoblotted with rabbit anti-GFP Ab followed by HRP-conjugated anti-rabbit IgG from a Rabbit IgG True Blot Kit (eBioscience). The sample was developed using ELC (Roche Applied Science).

Splenic DC isolation and cell culture

To isolate DC, spleens were placed in a petri dish with 1 mg/ml collagenase D and 100 μg/ml DNase I (Roche). The spleens were infused with collagenase D using a 1-ml syringe with a 25-gauge needle, cut into small pieces, and filtered through nylon mesh. Larger pieces of tissue that did not go through the nylon mesh were incubated in 5 ml of collagenase D/DNase I for 45 min at 37°C and filtered through nylon mesh again. The cells were spun at 200 $\times$ *g* for 10 min at 4°C and washed twice. Cells were resuspended in PBS (Life Technologies) plus 0.5% BSA (Sigma-Aldrich) and 2 mM EDTA (Life Technologies), Fc receptors were blocked with 2 mg/ml mouse Ig (Sigma-Aldrich) for 15 min at 4°C, and CD11c beads (Miltenyi Biotec) were added for an additional 15 min at 4°C. Cells were washed once and purified using an LS column (Miltenyi Biotec). Purified CD11c$^+$ DC were plated in petri dishes in the presence of 12.5 μg/ml LPS (Sigma-Aldrich) and 1 μg/ml anti-CD40 (BD Biosciences). After 16–18 h, cells in suspension were collected, separated on a Ficoll-Hypaque gradients (>1.033 g/ml), and washed twice with medium.

OT-II $\times$ Rag$^{-/-}$ TCR Tg splenocytes were activated in RPMI 1640 (Invitrogen) medium supplemented with 10% FBS (HyClone), nonessential amino acids, L-glutamine, sodium pyruvate (Mediatech) plus 2 μM of 2-ME (Sigma-Aldrich) in the presence of 5 μM OVA peptide. T cells were used on days 5–8 after activation. CD80-eYFP I-E^k Chinese hamster ovary (CHO) cells and 5C.C7 TCR Tg T cell activation has been previously described (12).

Intracellular staining for FoxP3

Lymph node suspensions were first stained with CD4-FITC and CD25-allophycocyanin. Stained cells were then fixed and permeabilized in BD Cytofix/Cytoperm (BD Biosciences) for 30 min at 24°C with 1% paraformaldehyde, 0.5% Tween 20, and stained with FoxP3-PE for 1 h at 24°C. All Abs were purchased from BD Biosciences.

Immunofluorescent staining and flow cytometry

For anti-Golgi staining, Ab clone 53FC3 against mannosidase II (Covance Research Products) was used at a 1/10,000 dilution with a goat anti-mouse secondary Alexa Fluor 488 conjugated (Invitrogen). For microtubule staining, cells were fixed with 2% paraformaldehyde in PBS at 37°C for 30 min and washed three times with PBS/human serum albumin. Cells were permeabilized with 0.1% Triton X-100 for 5 min at 24°C, washed three times, blocked with 5% goat serum in PBS for 1 h, and stained with 20 μg/ml anti-β-tubulin, clone TUB 2.1(Sigma-Aldrich), for 1 h at 24°C. Ab was diluted in staining buffer, 10% FBS, and 0.1% Tween 20 in PBS. Cells were washed three times and goat anti-mouse secondary Ab (Molecular Probes) was added at 1/250 for 30 min at 24°C and washed three times.

For Immunofluorescent staining and flow cytometry, allophycocyanin-conjugated anti-CD80 (1610A), anti-CD3ε, and anti-CD86 were purchased from eBioscience. Anti-CD28 (14-4-4s) and anti-CTLA-4 were purchased from BD Biosciences and anti-PKCθ polyclonal Ab was purchased from Santa Cruz Biotechnology. Alexa Fluor 546- conjugated secondary goat anti-Syrian hamster and goat anti-rabbit were purchased from Molecular Probes and Cy5- conjugated goat anti-Armenian hamster and anti-mouse were purchased from Jackson ImmunoResearch Laboratories. For acute blocking assay, anti-CD11c and anti-I-A^b Abs were purchased from BD Biosciences.

Microscopy and image analysis

For T cell-DC interaction, glass-bottom chambers were coated with 50 μl of 200 μg/ml human fibronectin (Fisher Scientific) for 1 h and washed twice with sterile H_2O. CD11c$^+$ purified and overnight-activated DC in serum-free medium were plated onto the glass chamber for 1 h at 37°C with 5% CO_2, and medium with OVA peptide was added for an additional 2 h. Days 5–8 after activated or naive OT-II $\times$ Rag$^{-/-}$ T cells were then added to the glass-bottom chambers for 30 min and fixed as described above. For live cell images, H57-F(ab′)$_2$-Alexa Fluor 568 or H155-F(ab′)$_2$-Alexa 568 (H57 and H155 are nonblocking Abs to TCR and LFA-1, respectively) were used.

For fixed cell images, samples were prepared as follows: after T cells-CHO cells interacted for 10–15 min at 37°C and 5% CO_2 in a Lab-Tek II Chamber 1.5 German Cover Glass System, 8-well glass-bottom slides (Nalge Nunc International), they were briefly washed with PBS to remove

excess T cells that failed to conjugate with the CHO cells. Sample were then fixed at 24°C with 4% methanol-free formaldehyde/PBS for 10 min (for permeabilized membrane) or with 2% methanol-free formaldehyde/PBS for 2 min (for nonpermeabilized membrane). The cells were washed three times with HBSS and incubated with primary Abs for 1 h at room temperature, washed, blocked with goat serum overnight at 4°C, and followed by secondary Abs for 1 h at 4°C.

For calcium imaging, OT-II T cells were labeled with 3 μM Fluo-LOJO (K_{Ca}^{2+} = 440 nM) for 30 min at 24°C in 1 ml of serum-free medium, washed twice, resuspended in medium with 10% serum. and incubated for 30 min at 37°C. Images of different fields were taken 5 min after adding T cells to DC, Alexa Fluor 647-conjugated H155 Fab and Alexa Fluor 568-conjugated H57 Fab. The 5-min time point was used as the standard observation point for T cell-DC interactions. Subsequently, anti-I-A^b (30 μg/ml) was added and images were collected every 4–5 min. Fluo-LOJO-loaded T cell anti-MHC isotype control (30 μg/ml) were imaged as control for photobleaching. LFA-1, CD80, and TCR cluster fluorescent intensity were measured at the interface using Image J (National Institutes of Health) before and after anti-MHCp treatment. Data analysis was done in Metamorph 5.0 (Universal Imaging) and Image J (National Institutes of Health).

Images were taken with an LSM 510 laser scanning confocal microscope (Zeiss) and ×100 PLAN Apochromat objective having a numerical aperture of 1.4. Image stacks consisted of 8–15 planes spaced by 0.48 μm. The images were analyzed using LSM (Zeiss) and Volocity (Improvision). For three-dimensional (3D) visualization of intercellular contacts, only those complexes were taken into consideration whose contact areas were oriented properly to be contained in a rectangular volume for an en face projection. Quick-time virtual reality (qtvr) allows multiple angle of 3D viewing of images.

Bilayer

Supported planar bilayers were formed using unilamellar liposomes containing Cy5-ICAM-1-GPI at 200 molecules/μm^2 and Ni^{2+} chelating 1, 2-dioleoyl-*sn*-glycero-3-succinyl-nitriloacetic acid (DOGS-NTA; Avanti Polar Lipids) to allow attachment of 6His-tagged soluble I-A^b. I-A^b-6His-$OVA_{323–339}$ was expressed in S2 insect cells and purified by immunoaffinity chromatography using a mAb to I-A^b (M5/114) coupled at agarose. The $OVA_{323–339}$ peptide (ISQAVHAAHAEINEAGR) was covalently linked to the β-chain of I-A^b. Varying concentrations of I-A^b were applied to planar bilayers containing 10% NTA lipids to generate different site densities. The concentration necessary to generate each site density was quantified by FACS using FITC-labeled M5/114 with calibration using FITC standard beads (Bangs Laboratories). All components were >80% mobile in the final bilayer preparations.

Previously activated day 6 OT-II TCR Tg T cells were loaded onto bilayers and fixed after 15 min with 2% paraformaldehyde. They were then permeabilized with 0.05% saponin. TCR was visualized by Alexa Fluor 568-H57 anti-TCR Fab and PKCθ was visualized with a rabbit polyclonal anti-PKCθ Ab from Santa Cruz Biotechnology and an Alexa Fluor 488-goat anti-rabbit $F(ab')_2$.

Bilayer imaging was performed using wide-field fluorescence or total internal reflection illumination on an Olympus microscope with a PLAPO ×60 with a 1.45 numerical aperture objective (Olympus America). Images were acquired using an Orca-ER (Hamamatsu) camera with a pixel size of 0.2 μm. Images were acquired using IPLab software, background was subtracted using Image J, and analyzed using Metamorph.

Statistical analysis

Pearson's correlation coefficient (r) was used to determine the degree of colocalization, segregation, or no correlation of the CD80, CD28, and PKCθ clusters in the IS (25). Pearson's correlation coefficient (R_r) is one of the standard techniques applied in pattern recognition for matching one image to another to describe the degree of overlap between the two patterns. In Pearson's correlation, the average pixel intensity values are subtracted from the original intensity values. As a result, the value of this coefficient ranges from −1 to 1, with a value of −1 representing a total lack of overlap between pixels from the images, and a value of 1 indicating perfect image registration. Pearson's correlation coefficient accounts only for the similarity of shapes between the two images and does not depend upon image pixel intensity values.

A single sample t test was performed to establish whether the correlation coefficient mean value is significantly different from zero. The Fisher exact test was used to determine whether the pattern accumulation is associated with wild-type (WT) DC and CD80-eCFP DC. The multinomial test for equal probabilities was used to determine whether there is a difference among CD80 accumulation patterns. The exact binomial test was used to determine whether the proportion of CD80-eCFP response to anti-MHC Ab treatment by the lost of clustering is the same as the group of no effect. Fisher's exact test was used to determine whether the difference in CD80 cluster loss by anti-MHC and anti-CD11c treatment is significant. The paired t test (after natural log transform on the data) and the Wilcoxon-signed rank test were used to determine whether there exists a difference in fluorescent intensity before and after anti-MHC Ab treatment of Ca^{2+}, LFA-1, CD80, and TCR fluorescence.

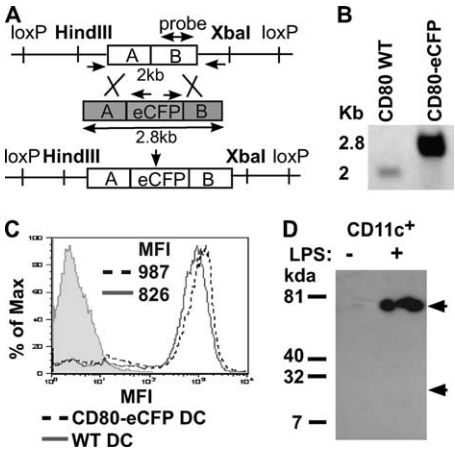

FIGURE 1. *CD80-eCFP* BAC transgene construction. *A*, A schematic of the BAC Tg construct map. RP23-69GS BAC clone containing *CD80* genomic DNA was recombined with shuttle vector (shaded gray) containing in-frame *eCFP* insertion before *CD80* stop codon to generate *CD80-eCFP* BAC transgene. *B*, Assessment of *eCFP* recombination into *CD80* genomic DNA BAC clone by Southern blot. *CD80* BAC WT and *CD80-eCFP* BAC Tg DNA were digested with *Hin*dIII and *Xba*I restriction enzymes. Positive *eCFP* insertion increased DNA molecular mass to 2.8 kb as compared with WT of 2 kb. *C*, Analysis of CD80-eCFP expression from BAC Tg. $CD11c^+$ splenic DC were isolated from BAC Tg on CD80/$CD86^{+/-}$ (dashed line) or WT (solid line) and matured for 16 h with LPS/anti-CD40. The mature DC were stained with anti-CD80 or isotype control (shaded) mAb and analyzed by flow cytometry. *D*, Relative molecular mass of CD80-eCFP. Anti-GFP Ab was used to immunoprecipitate and immunoblot LPS/anti-CD40-treated and untreated $CD11c^+$ splenic DC lysates. Immunoprecipitated samples were separated on a reducing 10% SDS-PAGE gel. A single band of 75 kDa was detected in a magnetic bead-selected $CD11c^+$ population treated with LPS/anti-CD40. LPS/anti-CD40 indicates in vitro treatment for 16 h with both 12.5 μg/ml LPS and 1 μg/ml anti-CD40. MFI, Mean fluorescent intensity.

Results

CD80-eCFP BAC Tg DC characterization

To study the dynamics of CD80 clustering in the IS between primary T cells and DC, we generated BAC Tg mice that expressed a CD80-eCFP chimera under control of *CD80*'s endogenous promoter. *Escherichia coli* containing BAC clone RP23-69GS were purchased from the National Center for Biotechnology Information. This clone spans a 185-kb chromosome insert containing the complete *CD80* gene near its center. The *CD80* gene was cloned into a shuttle vector and *eCFP* appended to the end of the cytoplasmic tail by overlapping PCR. Homologous recombination between the shuttle vector and the purified BAC DNA RP23-69GS was performed in *E. coli* (Fig. 1*A*). Positive clones containing *CD80-eCFP* in RP23-69GS were confirmed by PCR and Southern blot, in which digestion with *Hin*dIII and *Xba*I produced a fragment size of either 2 kb from the WT BAC or 2.8 kb from the recombinant BAC encoding *CD80-eCFP* (Fig. 1*B*). The *CD80-CFP* band appeared stronger than the endogenous *CD80* band due to the different amount of DNA loaded. *CD80-eCFP* BAC DNA was purified from *E. coli* and the size and integrity were confirmed

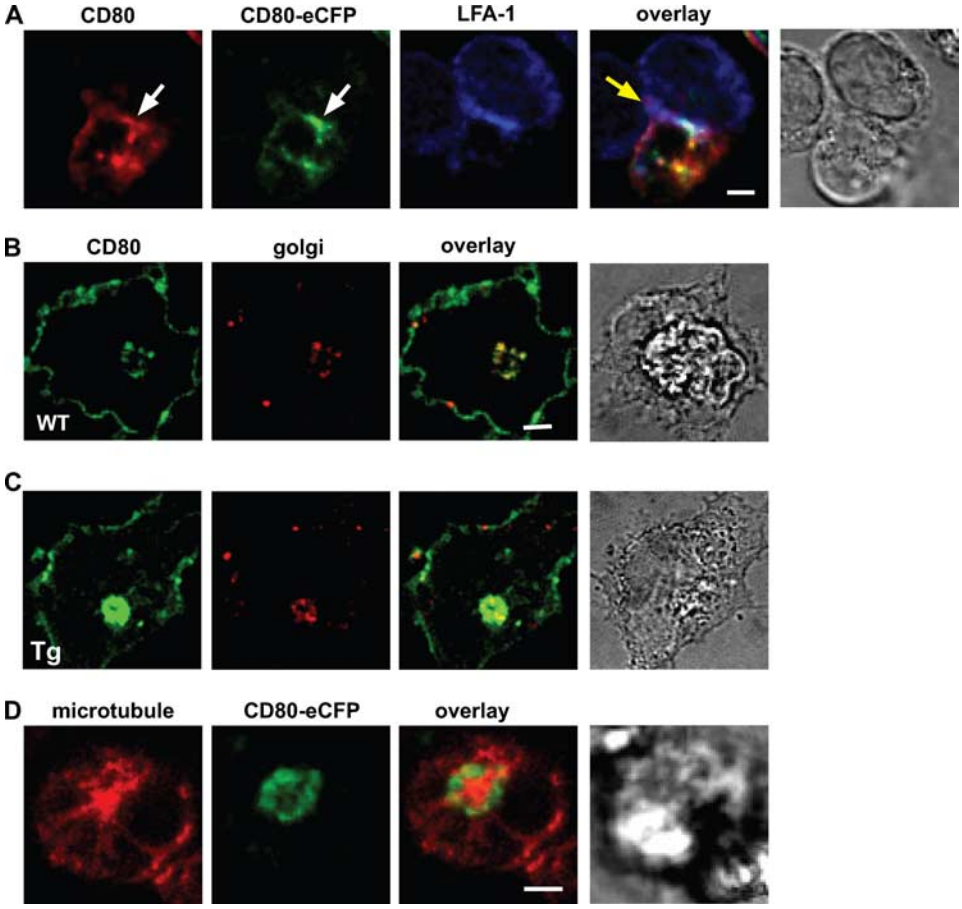

FIGURE 2. Characterization of CD80-eCFP spatial localization in CD11c$^+$ splenic DC. *A*, CD80-eCFP from BAC Tg × CD80/CD86$^{-/-}$ colocalized with CD80 WT in the T cell-DC IS. CD80 WT and CD80-eCFP BAC Tg (green) were stained with anti-CD80 (red), and the T cell was stained with anti-LFA-1 Fab (blue). This is a side view of the IS. Yellow area depicts CD80 and CD80-eCFP colocalization and white area depicts CD80, CD80-eCFP, and LFA-1 colocalization. White arrow bar indicates CD80 accumulation in the IS, and yellow arrow bar indicates T cell-DC interface. *B–C*, CD80 accumulated in the Golgi compartment. CD80 WT and CD80-eCFP BAC Tg were stained with anti-CD80 (green) and anti-Golgi (red). Yellow areas depict CD80 and Golgi colocalization, WT DC (*B*), and CD80-eCFP BAC Tg DC (*C*). *D*, Intracellular CD80-eCFP accumulated in the periphery of the MTOC. CD80-eCFP is shown in green and β-tubulin in red. CD11c$^+$ splenic DC were matured overnight with LPS/anti-CD40. Bar, 2 μm.

by pulse-field gel electrophoresis before injection into C57BL/6 oocytes to generate Tg mice (data not shown).

Tg founders were crossed to CD80/CD86$^{-/-}$ mice on the C57BL/6 background (26) and screened for total CD80 expression on mature DC relative to WT mature DC. Tg founders with similar total *CD80* (with one WT CD80 allele and one *CD80-eCFP* allele) to WT DC would have physiological expression from the CD80-eCFP BAC Tg. We obtained one founder in which CD11c$^+$ splenic DC matured in vitro had a similar mean fluorescent intensity after anti-CD80 staining, 987 for CD80-eCFP BAC Tg × CD80/CD86$^{-/+}$ vs 826 for WT (Fig. 1*C*). We then confirmed that eCFP was indeed fused to CD80 to generate a 75-kDa protein in mature CD11c$^+$ spleen cells via anti-GFP immunoprecipitation, SDS-PAGE, and detection by immunoblotting with anti-GFP Ab (Fig. 1*D*). There was no evidence of proteolytic generation of eCFP, which would have a relative molecular mass of 25 kDa. We were not able to detect CD80-eCFP on unstimulated CD11c$^+$ spleen cells consistent with expected induction of CD80 on DC maturation (Fig. 1*D*).

We determined whether CD80-eCFP expression and accumulation pattern during a T cell-DC interaction followed that of the endogenous CD80. Splenic CD11c$^+$ DC were matured overnight with LPS/anti-CD40 and then pulsed with 5 μM OVA peptide. OT-II TCR Tg T cells labeled with Alexa Fluor 633-conjugated anti-LFA-1 (H155 clone, nonblocking) Fab were added to these DC and fixed at 30 min. The DC were obtained from *CD80-eCFP* BAC Tg mice that were heterozygous for endogenous *CD80* and CD86. Anti-CD80 staining colocalized with the eCFP fluorescence in the IS (Fig. 2*A*). We noticed that there were intracellular accumulations of *CD80* in the DC and hypothesized that this was associated with the Golgi apparatus. To test this. we performed colocalization experiments with mannosidase II, a marker for the *cis*-face of the Golgi apparatus. Anti-CD80 mAb staining colocalized with anti-mannosidase II Ab staining in both the WT DC (Fig. 2*B*), and CD80-eCFP BAC Tg × CD80/CD86$^{-/-}$ DC (Fig. 2*C*). We further characterized the intracellular pool of CD80 accumulation in relation to the microtubule-organizing center (MTOC) by staining with anti-β-tubulin. We found that intracellular CD80-eCFP was closely apposed to the MTOC (Fig. 2*D*) in mature CD11c$^+$ DC, consistent with Golgi localization. In subsequent experiments, we use the Golgi-associated CD80 fluorescence for orientation in the DC and excluded the Golgi-associated CD80 fluorescence from analysis of CD80 clusters in the IS.

CD80-eCFP BAC transgene is functional

To demonstrate functional reconstitution of costimulation by the *CD80-eCFP* BAC transgene, we exploited the observation that mice deficient in both CD80 and CD86 molecules have a greatly

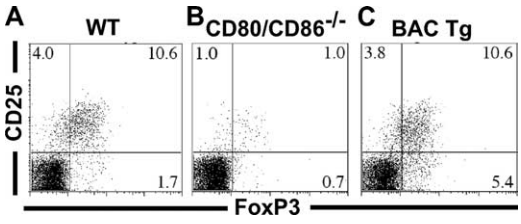

FIGURE 3. CD80-eCFP rescues Treg development in mice deficient in CD80 and CD86. Flow cytometry profile of CD25 and FoxP3 staining of CD4$^+$ lymph node cells from WT (*A*), CD80/86$^{-/-}$ (*B*), and CD80-eCFP BAC Tg × CD80/86$^{-/-}$ (*C*).

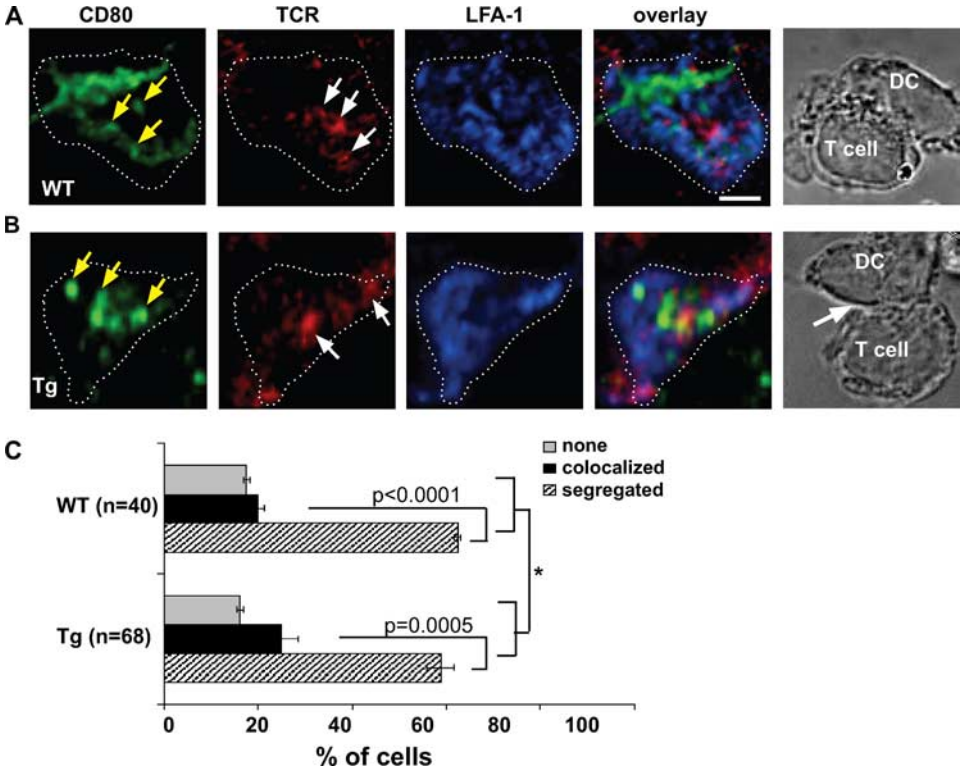

FIGURE 4. TCR and CD80 are segregated in the IS of CD11c$^+$ splenic DC. *A* and *B*, Image of T cell-DC IS. Overnight LPS/anti-CD40-matured WT (*A*) and CD80-eCFP (*B*) DC pulsed with 5 μM OVA were fixed (nonpermeabilizing conditions) for 30 min after adding OT-II T cells and stained with nonblocking Abs to TCR (H57) and LFA-1 (H155). The distribution of molecules was analyzed in at least two independent experiments in WT and CD80-eCFP. CD80 is shown in green, TCR in red, and LFA-1 in blue. Images are a cross-section of a 3D plane rotated in an en face view. Dotted white line depicts the interface of the IS. Yellow arrows depict cluster of CD80 accumulations and white arrow depicts cluster of TCR accumulations. The transmitted light image depicts a side view of T cell-DC conjugate. Bar, 2 μm. *C*, Quantification of CD80 accumulation patterns with respect to the TCR of *A* vs *B* in the IS over a 30-min time point. WT is shown in black and CD80-eCFP in gray. CD80 clusters segregated from TCR clusters were scored as segregated and CD80 clusters colocalized with the TCR clusters partially or entirely were scored as colocalized. When there were no CD80 clusters in the interface, these were scored as none. The difference in molecular accumulation between segregated and colocalized is extremely statistically significant with a p value of 0.0001 and 0.0005 for WT and CD80-eCFP, respectively, using a multinomial test for equal probabilities. *, The patterns of molecular segregation were not significantly different between WT and CD80-eCFP expressing DC, $p = 0.850$ using Fisher's exact test.

reduced regulatory T cell (Treg) population (27, 28). T cells from the lymph nodes of CD80-eCFP BAC Tg × CD80/CD86$^{-/-}$ mice were examined for Tregs by flow cytometry based on CD25 and FoxP3 expression. As seen in Fig. 3, ~10% of the CD4$^+$ T cells were double positive for CD25 and FoxP3 in both WT (Fig. 3*A*) and CD80-eCFP BAC Tg × CD80/86$^{-/-}$ (Fig. 3*C*), but only ~1% were double positive in CD80/86$^{-/-}$ (Fig. 3*B*). This demonstrates that one allele of the *CD80-eCFP* BAC Tg is functional in maintaining Tregs in vivo. Thus, CD80-eCFP functions similarly to WT CD80 and validates its use for IS studies.

Similar patterns of CD80-eCFP and WT CD80 in multifocal T cell-DC IS

We have previously shown that CD80-eCFP or CD80 WT colocalized with CD28 and CTLA4 in model IS formed between T cells and MHCp expressing CHO cells, but were mainly segregated from TCR clusters (12). Since the location of CD80 clusters and its relation to TCR clusters in the T cell-DC IS has not been determined, we first performed fixed immunofluorescence analysis to compare the pattern formed by CD80 WT to that formed by CD80-eCFP BAC Tg. We evaluated the localization of CD80 in relation to the TCR in the conjugates formed between OT-II T cells and WT DC or CD80-eCFP BAC Tg × CD80$^{+/-}$/86$^{-/-}$ (CD80-eCFP) DC. Immunofluorescence staining for CD80 and TCR was performed with conjugates fixed after coincubation for 30 min at 37°C. Three accumulation patterns were scored for >40 fixed cell contacts for each DC type in two independent experiments. CD80 clusters segregated from the TCR clusters were scored as segregated and CD80 clusters colocalized with the TCR clusters partially or entirely were scored as colocalized. When there were no CD80 clusters in the interface, these were scored as none, which may reflect no CD80 redistribution or redistribution at a level that cannot be distinguished from the basal CD80 at the plasma membrane.

Both WT DC (Fig. 4*A*; see supplemental qtvr 1 for 3D views)[5] and CD80-eCFP DC (Fig. 4*B*; see supplemental qtvr 2 for 3D views) had CD80 clusters (solid yellow arrow) that were segregated from the TCR clusters (solid white arrow) in 63% (SD = 0.7%) and 59% (SD = 2.8%) of IS, respectively. In contrast, only 20% (SD = 1.4%) and 25% (SD = 3.5%) of the time did CD80 colocalize with TCR, respectively (Fig. 4*C*). CD80 and TCR clusters were considered segregated when >50% of the CD80 clusters had no overlap with TCR clusters. We previously reported similar finding in the T cell-CHO cell model system (12). Unlike the IS formed with the CHO cell bilayer and B lymphoma presenting MHCp, a central TCR cluster was rarely observed in the T cell-DC IS.

[5] The online version of this article contains supplemental material.

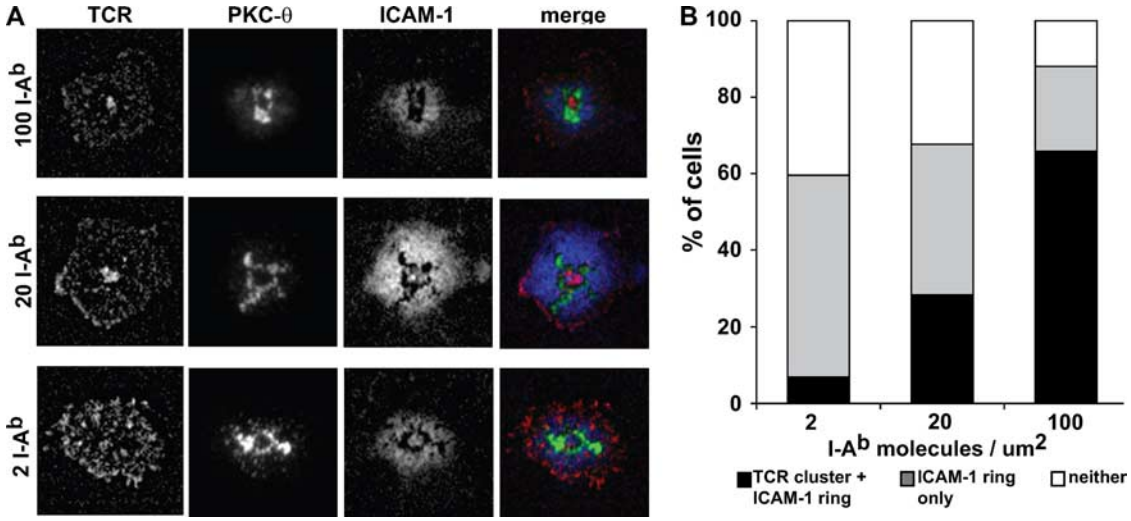

FIGURE 5. OT-II T cells formed defined cSMAC and pSMAC in the supported planar bilayer system. *A*, The supported planar bilayers were armed with 2, 20, or 100 I-A^b-OVA$_{323–339}$/μm^2 and fixed densities of Cy5-ICAM-1-GPI and CD80-GPI. The OT-II effector T cells were allowed to interact with the bilayers at 37°C and fixed at 15 min. TCR was followed with Alexa Fluor 568-H57 and PKCθ was detected with a rabbit antisera after fixation and permeabilization. In the merged images, TCR is shown in red, PKCθ is shown in green, and ICAM-1 is shown in blue. Bar, 5 μm. *B*, Quantification of OT-II T cell-bilayer IS pattern formation. All contacts could be categorized as having a central TCR cluster + the ICAM-1 ring, an ICAM-1 ring only, or neither. The χ^2 test gave a $p < 0.0001$ for the I-A^b-OVA$_{323–339}$ concentration dependence of the patterns.

Statistical analysis was performed to ask whether the IS patterns formed by WT DC vs CD80-eCFP DC are different. Fisher's exact test from two independent experiments gave a p value of 0.521 and 0.787, respectively, and a combined p value of 0.850, suggesting no difference between accumulation patterns in IS of T cell-WT DC and T cell-CD80-eCFP DC. Additional statistical testing was performed to ask whether the CD80 clusters were segregated from the TCR clusters significantly more than CD80 clusters colocalized with the TCR cluster. Using the multinomial test for equal probabilities, in the T cell-WT DC IS, individual experiments have p values of 0.011 and 0.036, respectively, and a combined p value of 0.0005. In the T cell-CD80-eCFP DC IS, individual experiments have p values of 0.044 and 0.0002, respectively, and a combined p value < 0.0001. Thus, the results indicate that CD80-eCFP expressing DC form similar molecular patterns in the IS as WT DC and that the molecular segregation of CD80 clusters from TCR clusters in the IS is statistically significant. These results suggest that the multiple close contacts observed in recent electron microscopy studies may represent distinct TCR clusters and CD80 clusters (17).

OT-II TCR Tg CD4 T cells form defined cSMAC and pSMAC

To determine whether the failure to observe a well-defined pSMAC and cSMAC in the OT-II T cell-DC IS is a property of the OT-II TCR system or a function of DC, we used the supported planar bilayer system. The supported planar bilayer system has previously been shown to fully reconstitute cSMAC formation similarly to B cells. The I-A^b-OVA$_{323–339}$ was attached to supported planar bilayers at 2, 20, or 100 molecules/μm^2. The OVA$_{323–339}$ peptide binds to I-A^b in three different registers such that <10% of the complexes are ligands for the OT-II TCR and thus we used 10-fold higher pMHC densities than we previously used for I-E^k-MCC$_{91–103}$, which binds in a single register. We included ICAM-1 and CD80 in the supported planar bilayers to enable pSMAC and cSMAC formation, respectively. Fig. 5 shows representative IS formed by previously activated OT-II T cell-formed IS with pSMAC and cSMACs in an I-A^b-OVA$_{323–339}$ dose-dependent manner ($p < 0.0001$, χ^2 test). I-A^b-OVA$_{323–339}$ at 0.2 molecules/μm^2 did not induce any TCR clustering or ICAM-1 rings. As previously described, the lowest density of MHCp that induced activation did not produce a significant TCR accumulation in the cSMAC, but did generate an ICAM-1 ring and PKCθ clustering in a single central structure. When 10–50 times higher densities of I-A^b-OVA$_{323–339}$ were used, a single central TCR accumulation was observed. It is notable that even in the supported planar bilayer system the TCR cluster in the cSMAC was segregated from the PKCθ cluster, which often formed a well-defined ring between the central TCR cluster and ICAM-1 ring. Based on precedents defined by Kupfer and colleagues (9), we would refer to the central TCR clusters and tightly apposed PKCθ ring as together comprising the cSMAC. In our analysis of T cell-DC IS, we used MHCp doses that are >10-fold over the threshold for T cell activation. Under these conditions, the OT-II T cells were capable of forming a single, well-defined cSMAC with a planer bilayer, but we have shown that they instead formed distinctly multifocal IS with activated splenic DC.

T cell-DC form a stable IS

We next wanted to take advantage of the CD80-eCFP DC to perform real-time imaging of T cell-DC interfaces to determine whether these were stable IS. OT-II T cells interacting with CD80-eCFP DCs were imaged by 3D confocal microscopy in which each 3D data set required ~10 s to acquire, and 3D data sets were acquired of the same conjugates at intervals of 30–120 s. The time series started 5 min after adding T cells to OVA peptide-pulsed mature CD11c$^+$ splenic DC. The TCRs were visualized on live T cells by staining with Alexa Fluor 547-labeled anti-TCRβ (H57 clone, nonblocking) Fab, which was maintained at a low concentration of 1 μg/ml in the coculture during imaging to maintain staining. The series of 3D projections revealed that the T cells remained with the same OVA peptide-pulsed DC (Fig. 6*A*) for the entire imaging period up to 10 min, even though the pattern of CD80 and TCR clusters changed over this time (Fig. 6*B*; see supplemental qtvr 3 and 4 for 3D views and supplemental movie 1).

Although the pattern of the CD80 and TCR clusters in the IS changed overtime, CD80 and TCR remained segregated. The degree of CD80 and TCR cluster segregation over time in Fig. 6*B* were

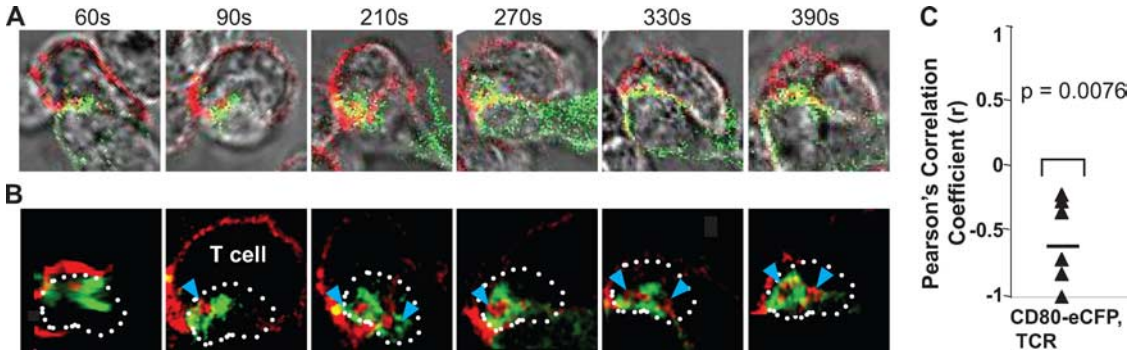

FIGURE 6. Dynamics of CD80 and TCR clusters in T cell-DC interface. A time series of Alexa Fluor 568-H57 Fab-labeled OT-II CD4$^+$ TCR Tg T cells interacting with mature CD80-eCFP DC. Time is relative to the first detected contact area at 60 s. *A*, Transmitted light images of T cell-DC conjugate. The fluorescence intensities of these images were enhanced to delineate the physical location of the T cell and DC. *B*, Cross-section of a 3-D plane rotated in an en face view. Dotted circles depict the interface of the IS. CD80 is shown in green and TCR is shown in red. Blue arrowheads depict cluster of TCR accumulation. This sequence is representative of two experiments with at least 10 cells. *C*, The degree of segregation between CD80 and TCR is represented by the mean Pearson's correlation coefficient *r*. One sample *t* test gave a $p = 0.0076$, suggesting that the *r* value is significantly different from zero and that CD80 and TCR are negatively correlated.

quantified by Pearson's correlation coefficient (*r*). The values of this coefficient range from -1 to 1. A value of -1 represents perfect segregation, a value of zero represents random localization, and a value of 1 represents perfect colocalization. For the interface of Fig. 6*B* time series, we obtained $r = -0.568$ with SE = 0.131 (Fig. 6*C*). Pearson's correlation coefficient accounts only for the similarity of shapes between the two images after application of a threshold and does not depend upon image pixel intensity values. To test the significance of the *r* value obtained, we asked whether CD80 and TCR clusters are negatively correlated. One sample *t* test gave a $p = 0.0076$, suggesting that the *r* value is significantly different from zero and that CD80 and TCR clusters are negatively correlated. These data are consistent with segregation of dynamic CD80 clusters and TCR clusters with overlap due to resolution limits of the imaging system.

CD80 is recruited to the IS by CD28

The question remains whether these CD80 clusters in the IS were bound by CD28. We have previously shown in the effector T cell-CHO cell system that CD28 and CD80 colocalized at 30 min (12). We used this system as a positive control here to demonstrate that

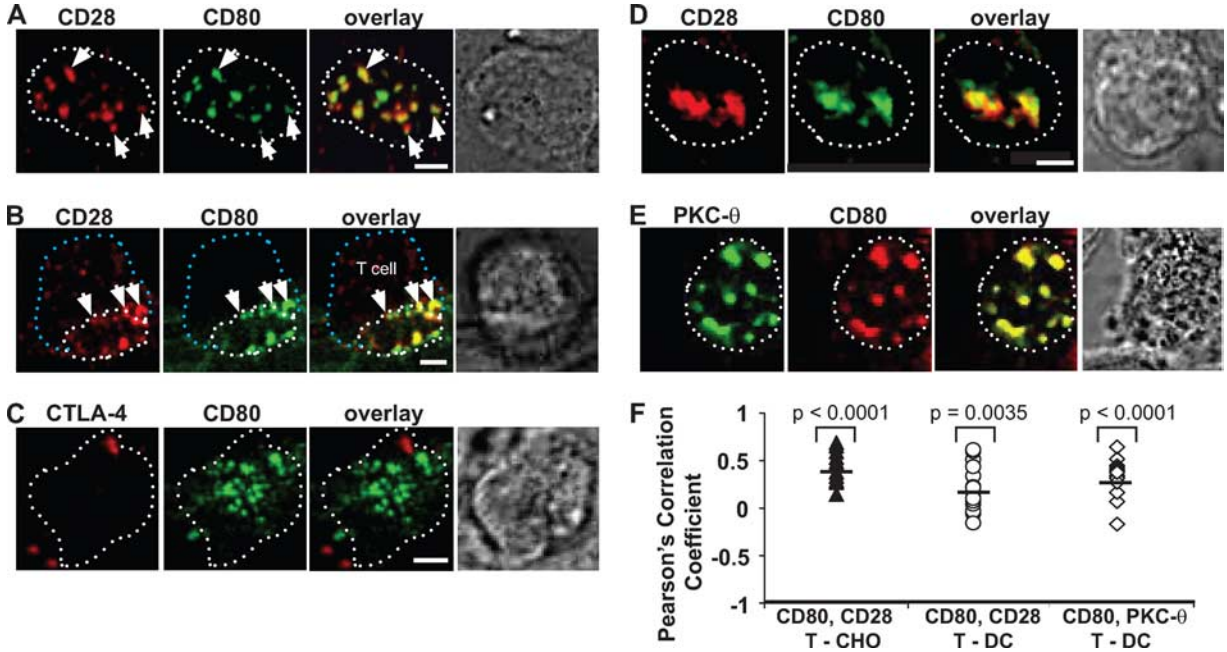

FIGURE 7. CD80 interactions with its ligands in the IS. T cell-CHO cell conjugates were fixed 15 min after adding 5C.C7 CD4$^+$ T cells. *A* and *B*, CD80 colocalized with CD28 in the IS. *A*, En face view of the T cell and CHO cell interface. *B*, Cross section of a semi-side view of a T cell and CHO cell conjugate. *C*, At this time point, CD80 colocalization with CTLA-4 was not detected in T cell and CHO cell interface. *D*, CD28 and CD80 colocalized in the T cell and DC interface of CD80-eCFP (CD80$^{-/+}$CD86$^{-/-}$) DC. *E*, CD80 clusters colocalized with PKCθ clusters in the T cell and DC interface of CD80-eCFP (CD80$^{-/+}$CD86$^{-/-}$) DC. *F*, Degree of colocalization represented by mean *r*. ▲, Represent *r* for CD80 and CD28 in the T cell-CHO cell IS. ○, Represent *r* for CD80 and CD28 in T cell-DC IS. △, Represent *r* for CD80 and PKCθ in the T cell-DC IS. One sample *t* test gave $p < 0.0001$, $p = 0.0035$, and $p < 0.0001$, respectively, suggesting that the *r* value is significantly different from zero and that these receptors are positively correlated. CD28, CTLA-4, and PKCθ are shown in red, CD80 in green, and colocalization in yellow. The dotted white circles represent the limits of the interface, the dotted blue circle represents the back of the T cell, and the white arrows depict cluster colocalization. Images were a cross-section of a 3D plane rotated in an en face view. Bar, 2 μm.

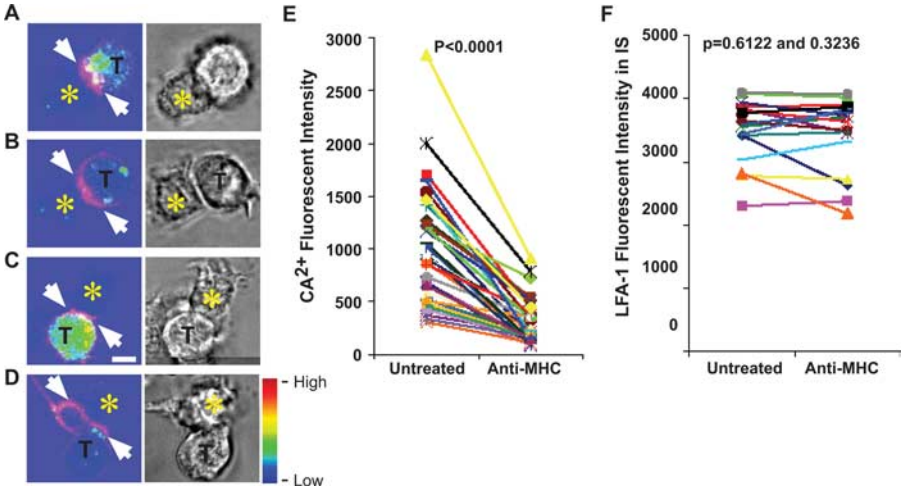

FIGURE 8. Acute disruption of TCR signaling decreased Ca^{2+} flux but not LFA-1 accumulation. *A–D*, Two examples of Fluo-LOJO (color coded)- and LFA-1 Fab (magenta)-labeled OT-II TCR Tg T cells (T)-DC (unlabeled, yellow asterisks) IS. Next to the fluorescent panels are the bright-field-transmitted light images of T cell-DC conjugates. *A* and *C*, Color-coded Ca^{2+} fluorescent images taken 5 min after T cell addition and before anti-MHC Ab treatment. *B* and *D*, Color-coded Ca^{2+} fluorescent images were taken 8 min after anti-MHC treatment. White arrows depict LFA-1 polarization before and after anti-MHC treatment. Bar, 5 μm. The rainbow scale indicates relative Fluo-LOJO fluorescent intensity. *E*, Quantification of Ca^{2+} flux as a measure of Fluo-LOJO fluorescent intensity. Conjugates were imaged before and every 4–5 min after anti-MHC treatment for up to 15 min. The difference in fluorescent intensity before and after anti-MHC treatment is statistically significant with a $p < 0.0001$ using the Wilcoxon-signed rank test and paired *t* test. *F*, Quantification of LFA-1 fluorescent intensity in the IS of T cells before and after anti-MHC treatment. The LFA-1 remained polarized after anti-MHC treatment. The difference in fluorescent intensity before and after anti-MHC treatment is not statistically significant with a *p* of 0.6122 and 0.3236 using the Wilcoxon-signed rank test and paired *t* test, respectively. The decrease in Ca^{2+} fluorescent intensity observed was analyzed in at least two independent experiments with $n > 35$ cells examined per experiment.

CD80-eYFP and CD28 are extensively colocalized in the T cell-CHO cell conjugates at 15 min (Fig. 7, *A* and *B*). Occasionally, we did observe CD80 clusters that did not have coassociated CD28 staining, but this was <10% of CD80-eYFP clusters. The degree of CD80-eYFP and CD28 cluster colocalization was quantified by the mean Pearson correlation coefficient, which was determined to be $r = 0.411$ ($n = 13$) with SE = 0.045 (Fig. 7*F*, ▲). We asked whether CD80-eYFP and CD28 clusters are positively correlated. One sample *t* test gave a $p < 0.0001$, suggesting that the *r* value is significantly different from zero and that CD80-eYFP and CD28 clusters are colocalized.

In the same system, there was no evidence for significant CTLA-4 clustering with CD80-eYFP at 15 min (Fig. 7*C*). The conjugates were fixed with a nonpermeabilized condition to ensure that only surface CTLA-4 was stained. Therefore, in the absence of CD86, CD28 preferentially bound to CD80 and these clusters participated in T cell activation as evidenced by their colocalization with PKCθ (data not shown). This is supported by our previous result where CD28, CD80, and PKCθ were colocalized at 30 min in effector T cell-CHO cell conjugates (12).

We then determined whether CD80 and CD28 are colocalized in the T cell-DC IS. The DCs used in these studies were CD80-eCFP BAC Tg × $CD80^{+/-}$/$CD86^{-/-}$. At the 15-min time point, CD80-eCFP and CD28 were colocalized in the IS (Fig. 7*D*). There was a relatively small area of CD28 accumulation that did not contain CD80-eCFP accumulation and the converse. This observation is consistent with extensive engagement of CD28 and CD80-eCFP where some component of CD28 and CD80-eCFP clustering is not strictly dependent upon a 1:1 receptor-ligand interaction. Nonetheless, CD80-eCFP clusters extensively colocalized with PKCθ staining in the T cell-DC IS (Fig. 7*E*), which is consistent with CD28-mediated signaling activity associated with each CD80-eCFP cluster even when equivalent CD28 clustering was not evident. The degree of CD80-eCFP and CD28 cluster colocalization (Fig. 6*F*, ○) and CD80-eCFP and PKCθ (Fig. 7*F*, △e) were quantified by Pearson's correlation coefficient, $r = 0.217$ ($n = 16$) with SE = 0.063 and $r = 0.315$ ($n = 13$) with SE = 0.048, respectively. We asked whether CD80-eCFP and CD28 clusters and CD80-eCFP and PKCθ are positively correlated, and one sample *t* test gave a $p = 0.0035$ and $p < 0.0001$, respectively. This suggests that the *r* values are significantly different from zero and that CD80-eCFP is colocalized with CD28 and PKCθ clusters.

Sustained TCR signals maintain CD80 accumulation in the IS

To study the relationship between TCR signaling and CD80 interactions in the IS, we set out to disrupt new TCR-MHCp interactions at defined times with a MHC-blocking Ab (29). We first tested whether anti-I-A^b can block TCR signal by labeling OT-II TCR Tg T cells with the Ca^{2+} sensitive dye Fluo-LOJO. OT-II T cells showed elevated Fluo-LOJO fluorescence within 5 min of introduction to OVA-pulsed DC (Fig. 8, *A* and *C*). This elevated fluorescence was reduced to basal levels within 4 min of anti-I-A^b (anti-MHC) Ab treatment (Fig. 8, *B* and *D*), as previously described in cellular systems (29). This is also similar to results on supported planar bilayers in which Ca^{2+} signaling is reduced to baseline within 2 min as the last TCR microcluster reach the cSMAC (13). We quantified Fluo-LOJO-labeled T cell fluorescence before and after anti-MHC treatment (Fig. 8*E*) and asked whether the reduction in fluorescent intensity is statistically significant. Both the Wilcoxon-signed rank test and the paired *t* test (after log transform) gave a $p < 0.0001$, demonstrating that the difference is statistically significant. This reduction in fluorescence was not due to photobleaching since the same number of imaging iterations produced no reduction in fluorescence when the cells were treated with a control Ab (data not shown) and the addition of ionomycin still increased Fluo-LOJO fluorescence after anti-MHC treatment (data not shown). No changes in fluorescence were observed in the absence of Fluo-LOJO dye. We also quantified LFA-1 fluorescence intensity before and after anti-MHC treatment in T cells that showed a Ca^{2+} reduction (Fig. 8*F*) and asked

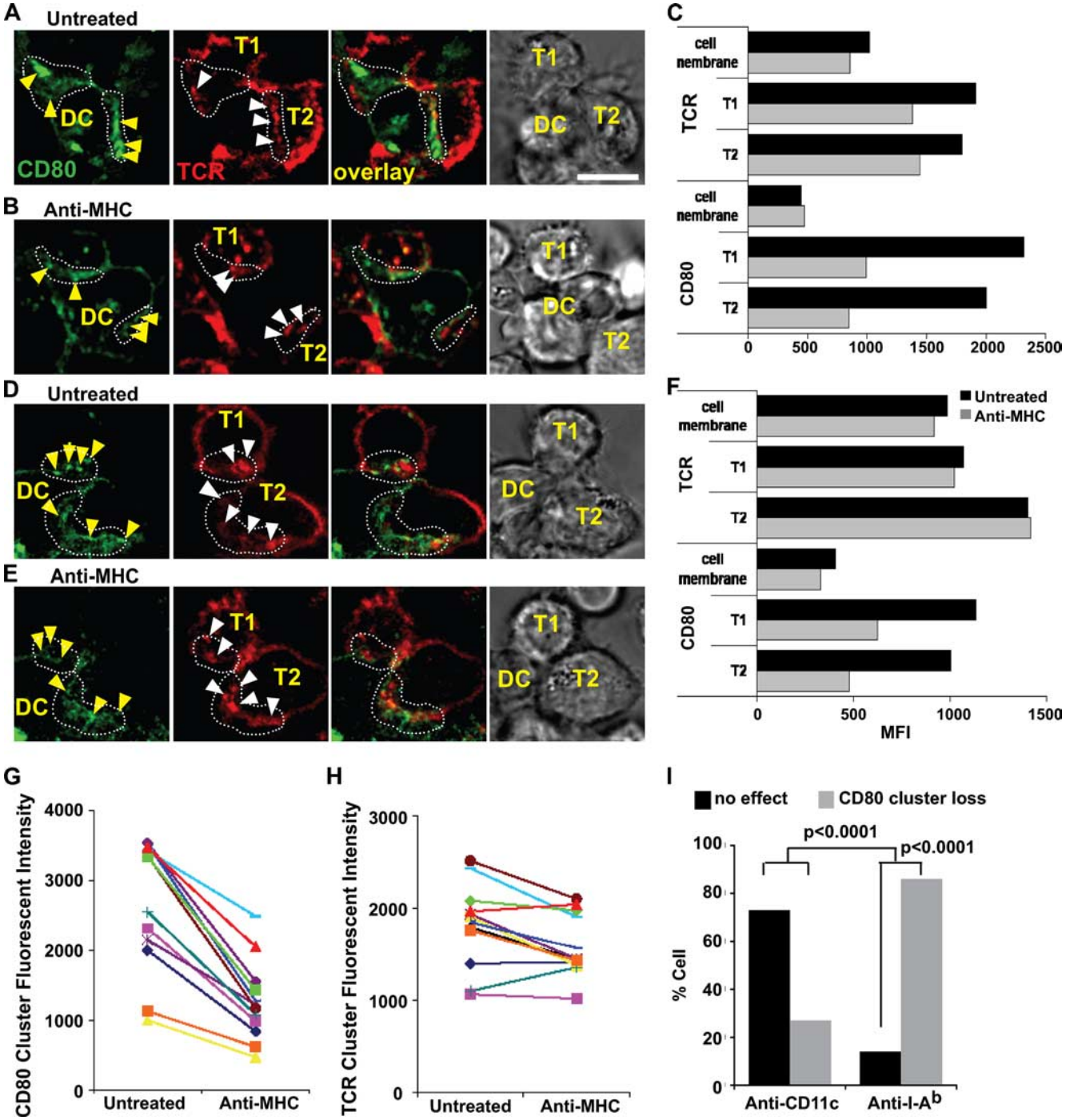

FIGURE 9. CD80 interaction in the IS is dependent on continuous TCR signaling. Images of untreated (*A* and *D*) and images of 10–15 min anti-MHC-treated T cell-CD80-eCFP (*B* and *E*) DC. *C* and *F*, mean fluorescence intensity of TCR and CD80 accumulation in the interface of T cell-DC untreated in *A* and *D*, respectively, and anti-MHC treated in *B* and *E*, respectively. Fluorescent intensity quantitation of CD80 (*G*) and TCR (*H*) clusters before and after anti-MHC Ab treatment in the T cell-DC IS. The difference in CD80 fluorescent intensity before and after anti-MHC treatment is statistically significant with a $p = 0.0004883$ and $p < 0.0001$ using the Wilcoxon-signed rank test and paired *t* test, respectively. The difference in TCR fluorescent intensity before and after anti-MHC treatment is statistically significant with a $p = 0.016$ and 0.0203 using the Wilcoxon-signed rank test and paired *t* test, respectively. $n = 12$ ISs were scored for CD80 and TCR fluorescent intensity before and after anti-MHC treatment. *I*, Quantitation of CD80 clusters loss in the T cell-DC IS after acutely blocking TCR signals. Anti-CD11c Ab was used as an irrelevant Ab control. The difference in cluster loss vs no effect after anti-MHC treatment is statistically significant with a $p < 0.0001$ using the exact binomial test. The difference in cluster loss vs no effect between anti-MHC and anti-CD11c treatment is statistically significant with a $p < 0.0001$ using the Fisher exact test. Conjugates were imaged every 4–5 min after anti-MHC treatment for up to 15 min. CD80 is shown in green and TCR in red. The distribution of molecules and loss in CD80 clusters were analyzed in at least three independent experiments with $n > 20$ cells examined per experiment. The yellow arrows indicate CD80 accumulation, and white arrowheads indicate TCR accumulation. Bar, 5 μm.

whether the change in LFA-1 fluorescent intensity is statistically significant. Statistical analysis using the Wilcoxon-signed rank test and the paired *t* test gave a $p = 0.6122$ and 0.3236, respectively. Thus, the change in LFA-1 fluorescent intensity after anti-MHC treatment is not significant. LFA-1 remained polarized toward the IS for at least 5 min, and the IS remained intact as previously described in the

T cell-B cell lymphoma model system (30). The LFA-1 staining was due to LFA-1 expression on T cells since LFA-1 expression on DC is not detectable with our image parameters.

In contrast, the treatment of T cell-DC IS with the anti-MHC Ab dramatically reduced CD80 clusters within 4 min (Fig. 9, *A*, *B*, *D*, and *E*). We quantified this result in two ways. First, we measured the CD80 fluorescent intensity at the interface before and after anti-MHC treatment using areas outside the IS for reference. A total of 12 interfaces were quantified and we found that the fluorescent intensity relative to the baseline was reduced 70–90% after anti-MHC treatment (Fig. 9, *C*, *F*, and *G*). We asked whether the difference in CD80 cluster fluorescent intensity before and after Ab treatment is statistically significant. Statistical analysis using the Wilcoxon-signed rank test and paired *t* test resulted in $p = 0.0005$ and $p < 0.0001$, respectively. Thus, the change in CD80 cluster fluorescent intensity after anti-MHC treatment is significant. We also scored 36 ISs for reduction in the number of CD80 clusters vs no affect on CD80 clusters after anti-MHC treatment (Fig. 9*I*). Our result suggests that 89% of the IS had CD80 cluster loss 4 min after anti-MHC treatment. We asked whether the loss of CD80 clusters vs no effect after anti-MHC treatment was statistically significant. Statistical analysis using the exact binomial test gave a $p < 0.0001$. In the irrelevant Ab control group, anti-CD11c treatment resulted in loss of CD80 clusters in 26% of the ISs, which we attributed to fluctuations in CD80 cluster number due to normal dynamics. We asked whether the difference in CD80 cluster loss between anti-MHC and anti-CD11c Ab treatment was significant. Statistical analysis using the Fisher exact test gave a $p < 0.0001$, demonstrating that significantly more clusters are lost after anti-MHC than with anti-CD11c treatment.

The anti-MHC treatment had a less dramatic effect on TCR accumulation. The fluorescent intensity of the TCR clusters in the IS was not dramatically reduced as compared with the CD80 clusters (Fig. 9, *C* and *F–H*). The TCR clusters continued to be dynamic with either no changes in fluorescence intensity (Fig. 9, *C* and *H*) or some decrease in fluorescence intensity of ~20–40% relative to the baseline (Fig. 8, *F* and *H*). Although there was a small decrease in TCR cluster fluorescence intensity compared with CD80 clusters, the difference in TCR clusters fluorescence intensity before and after anti-MHC treatment was statistically significant with $p = 0.016$ and 0.0203,respectively, using the Wilcoxon-signed rank test and paired *t* test. Our result shows that the loss of CD80-eCFP clusters was not due simply to loss of IS formation or IS stability, but the loss of continuous TCR signaling. Thus, the maintenance of CD80-CD28 interaction in the IS requires continuous TCR signaling.

Discussion

Organization of the T-DC IS

Our primary goal in this study was to advance knowledge of how TCR and costimulatory signaling are coordinated in the T cell-DC IS, an area that has not been studied. Our work builds on a substantial body of knowledge from model systems that have identified short-lived TCR microclusters and longer-lived cSMAC structures, both of which can associate with CD28-CD80 interactions that mediate an important component of costimulation. We used primary splenic DC purified from functionally validated BAC Tg mice in which CD80 is the only CD28 ligand and is labeled with eCFP. Our results provide insight into the organization of the T cell-DC IS and the dynamics of the CD80 clusters allows us to relate these to previously defined structures. We have found that the organization of CD80 clusters in the T cell-DC interface is most similar to that in T cell-transformed fibroblast (CHO) model systems (12, 31), more so than in T cell-B cell tumor systems, in that CD28-CD80 clusters are largely segregated from visible TCR clusters. Second, we found that CD80 clusters focus PKCθ in T cell-DC IS even though they are segregated from TCR clusters. We also found that the CD80 clusters are highly dynamic and require new TCR-MHCp interactions for maintenance, whereas the visible TCR clusters and LFA-1 clusters had greater "memory" for signals generated by new TCR-MHCp interactions. Thus, CD80 clusters have characteristics of microclusters in that they require recently established (within 4–5 min) TCR-MHCp interactions, but also share a characteristic with the cSMAC in that they are sites of PKCθ focusing in the IS.

We also verified that the multifocal TCR clusters observed between OT-II TCR Tg T cell and DC IS was not likely due to the inability of the T cells to form a cSMAC consisting of TCR clusters in the center of the IS with a suitable substrate. We found that OT-II T cells form a well-defined IS with supported planar bilayers that includes a cSMAC and pSMAC. As recently described for a different TCR system restricted by I-E^k, the cSMAC formed by the previously activated OT-II cells on bilayers with I-A^b-$Ova_{323–339}$ complexes, ICAM-1, and CD80 contains a readily resolved TCR-rich core surrounded by a ring of CD28 and PKCθ (32). These results suggest that T cells actively segregate TCR and PKCθ, but the failure to organize into a single cSMAC may be dependent on the DC.

Distribution and function of CD80-eCFP

One of the reasons that we chose to make BAC *CD80-eCFP* is because it has been shown that the expression of large DNA transgenes can accurately reflect the pattern of the endogenous chromosomal gene transcription (33). A major advantage of BAC Tg mice is that it allows the recombinant gene of interest to be under the control of its endogenous promoter, thus protecting its expression from position effect variegation. As a consequence of the size of BACs, a low copy number of concatamers is generally observed.

We found that CD80-eCFP is localized at the plasma membrane, but is also colocalized at the light microscopy level with the Golgi apparatus. The area around the centrioles is crowded with many vesicles; therefore, it is possible that the intracellular CD80 is associated with a distinct compartment from the Golgi. All type I transmembrane proteins that are expressed at the plasma membrane must traverse the Golgi apparatus (34). We did not perform an extensive comparison to other type I transmembrane proteins to determine whether this signal represents normal trafficking, retention in the Golgi or Golgi proximal compartments, or an intermediate in regulated secretion (33). Endogenous CD80 and CD80-eCFP displayed this localization to similar extents, demonstrating that this is not an effect of appending eCFP. We were surprised that we were unable to find any prior reference to CD80 localization near the Golgi apparatus, but most cell biology studies have focused on CD86 (35). Practically, this Golgi proximal signal is strong enough to require care in scoring of T cell-DC conjugates to make sure that the Golgi proximal staining is not misinterpreted as an IS- associated cluster.

Previous work has demonstrated an absolute requirement for either CD80 or CD86 for Treg maintenance in the periphery (27, 36). In contrast, CD80 and CD86 are not absolutely required for activation of conventional $\alpha\beta$ T cells by most Ags (37). Thus, the single most robust test for in vivo CD80 function was the ability to maintain peripheral Tregs. We showed that the *CD80-eCFP* transgene crossed to *CD80/CD86*$^{-/-}$ mice maintained peripheral Treg in normal numbers. This demonstrates that the expression pattern

and cell biology of CD80-eCFP is similar to that of endogenous CD80, although we did not determine whether CD80-eCFP fully replaces function of both CD80 and CD86 in immune responses. Nonetheless, the ability of CD80-eCFP to maintain Tregs demonstrates that it is functional in vivo.

Multiple TCR clusters in the OT-II T cell-DC IS

The OT-II T cell-DC IS contained many large TCR clusters that appeared to be scattered throughout the IS, consistent with recent reports (17). It is not clear whether these are structures involved in active signaling, postsignaling complexes, or a mixture of these. Our findings using OT-II Tg T cells and DC are distinct from earlier data that B lymphomas presenting suboptimal levels of MHCp induced multiple TCR clusters without a cSMAC (38), because we did not observe a cSMAC in T cell-DC IS at MHCp densities leading to maximal T cell stimulation with LPS/anti-CD40 matured DC. It is not clear whether the multifocal T cell-DC IS are due to distinct signals from DC surface molecules that direct the T cell cytoskeleton to general multiple TCR foci, due to resistance of the DC cytoskeleton to convergent movement by the T cell cytoskeleton, or due to specific characteristics of the OT-II TCR. The idea that the DC cytoskeleton plays an important role is consistent with observations that DC cytoskeleton contributes to T cell activation (39–41). Cytoskeletal restriction of MHCp and CD80 mobility on the DC may be important for DC to simultaneously maintain multiple ISs with different T cells without allowing the first IS formed to sequester resources from other IS (5, 42). However, treatments of DC with cytochalasin D and nocodazole before adding T cells did not disrupt the multiple TCR clusters observed in the T cell-DC interface (17). Further molecular analysis of different TCR Tg T cell systems and DC with higher spatial and temporal resolution is needed to answer these questions.

Segregation of TCR and CD80 clusters

We previously observed that CD80 clusters segregated from TCR clusters and were more peripheral compared with the TCR in IS formed between naive T cells and CHO cells engineered to express I-E^k and CD80 (12). This peripheral segregation correlates with enhanced costimulatory signals through CD28. Such peripheral segregation was not previously observed in T cell-B lymphoma or T cell-planar bilayer IS (21, 22), but it is possible that this is due to physical overlap of structures that are segregated on the molecular scale. Parallel studies with microcontact printing on solid substrates in which anti-CD3 and anti-CD28 Abs were presented in a unifocal colocalized pattern (cSMAC like), a multifocal segregated pattern, or a multifocal colocalized pattern demonstrate that multifocal CD28 engagement, not segregation of CD28 and TCR engagement, is the critical parameter for enhanced IL-2 production (47).

Dynamics of CD80 clusters

Our primary motivation for generating CD80-eCFP BAC Tg mice was to be able to study the dynamics relationship of CD80 interactions in relation to the TCR in a physiological IS. We first performed dynamic 3D imaging and then used blocking anti-MHC Abs to perturb the system. Dynamic 3D imaging demonstrated that CD80 clusters and TCR clusters are mobile in the IS. Krummel and colleagues (23) noted that TCR and CD28 tend to colocalize in the early stages of TCR microcluster formation. These observations led us to hypothesize that CD80 clusters are formed around early TCR clusters that are too faint to detect by conventional confocal imaging. We speculate that with time these clusters gain TCR, turn off TCR signaling, after which CD80 disperses, leaving a TCR-only cluster. A reciprocal relationship between TCR and CD80 has been observed in the cSMAC in T cell-planar bilayer systems (43). In the dynamic T cell-DC IS, this process rapidly leaves larger visible TCR clusters without associated CD80 interactions. This is one possible explanation for why visible TCR clusters are segregated from CD80 clusters. The CD80-eCFP BAC Tg mice provide an excellent reagent to pursue this hypothesis using higher speed 3D-imaging approaches.

Rapid response of CD80 declustering to cessation of early TCR signaling

Acute blockade of new TCR interactions with MHC- blocking Ab stops signaling within 4 min and eliminated CD80 clusters in the same time frame. Interestingly, TCR clusters decreased less and LFA-1 clusters were stable in this time frame. This suggests that these TCR clusters visible by confocal microscopy in the T cell-DC interface are more cSMAC-like and supports the idea that these are postsignaling complexes.

The persistence of the LFA-1 clusters for longer after cessation of new TCR-MHCp interactions than CD80 clusters was surprising. LFA-1 activity on resting T cells is regulated in minutes by TCR signals (44). Perhaps LFA-1 clusters generate their own positive feedback signals once engaged and thus can persist even when TCR signals are extinguished (45).

The rapid dispersal of the CD80 clusters following blockage of new TCR engagement is consistent with a model in which the CD80 clusters form in response to TCR-nucleated CD28 clustering. In CHO cells expressing CD80-eYFP, the Ag- dependent clustering of CD80 corresponded exactly to sites of CD28 and PKCθ clustering (12). The segregation of CD80 from TCR clusters was observed in most, but not all T cell-DC IS. The mechanism for segregation may be based on loss of signaling in larger TCR clusters leading to loss of associated CD28 clustering activity or the physical segregation of MHCp clusters from CD80 clusters by the DC. Addressing these questions will require new imaging technologies that combine super-resolution and speed (46).

Acknowledgments

We thank Dr. G. Eberl for advice on BAC Tg construction and Dr. J. Lafaille for help with the in vivo characterization of Treg cells. We thank Drs. T. Cameron and R. Varma for critical reading of this manuscript. We acknowledge the New York University Cancer Institute Biostatistics shared core facility.

Disclosures

The authors have no financial conflict of interest.

References

1. Delon, J., N. Bercovici, G. Raposo, R. Liblau, and A. Trautmann. 1998. Antigen-dependent and -independent $Ca2^+$ responses triggered in T cells by dendritic cells compared with B cells. *J. Exp. Med.* 188: 1473–1484.
2. Bousso, P., and E. Robey. 2003. Dynamics of $CD8^+$ T cell priming by dendritic cells in intact lymph nodes. *Nat. Immunol.* 4: 579–585.
3. Miller, M. J., O. Safrina, I. Parker, and M. D. Cahalan. 2004. Imaging the single cell dynamics of $CD4^+$ T cell activation by dendritic cells in lymph nodes. *J. Exp. Med.* 200: 847–856.
4. Shakhar, G., R. L. Lindquist, D. Skokos, D. Dudziak, J. H. Huang, M. C. Nussenzweig, and M. L. Dustin. 2005. Stable T cell-dendritic cell interactions precede the development of both tolerance and immunity in vivo. *Nat. Immunol.* 6: 707–714.
5. Mempel, T. R., S. E. Henrickson, and U. H. Von Andrian. 2004. T-cell priming by dendritic cells in lymph nodes occurs in three distinct phases. *Nature* 427: 154–159.
6. Dustin, M. L., M. W. Olszowy, A. D. Holdorf, J. Li, S. Bromley, N. Desai, P. Widder, F. Rosenberger, P. A. van der Merwe, P. M. Allen, and A. S. Shaw. 1998. A novel adaptor protein orchestrates receptor patterning and cytoskeletal polarity in T-cell contacts. *Cell* 94: 667–677.
7. Grakoui, A., S. K. Bromley, C. Sumen, M. M. Davis, A. S. Shaw, P. M. Allen, and M. L. Dustin. 1999. The immunological synapse: a molecular machine controlling T cell activation. *Science* 285: 221–227.
8. Wulfing, C., M. D. Sjaastad, and M. M. Davis. 1998. Visualizing the dynamics of T cell activation: intracellular adhesion molecule 1 migrates rapidly to the T

cell/B cell interface and acts to sustain calcium levels. *Proc. Natl. Acad. Sci. USA* 95: 6302–6307.
9. Monks, C. R., B. A. Freiberg, H. Kupfer, N. Sciaky, and A. Kupfer. 1998. Three-dimensional segregation of supramolecular activation clusters in T cells. *Nature* 395: 82–86.
10. Krummel, M. F., M. D. Sjaastad, C. Wulfing, and M. M. Davis. 2000. Differential clustering of CD4 and CD3ζ during T cell recognition. *Science* 289: 1349–1352.
11. Sanchez-Lockhart, M., E. Marin, B. Graf, R. Abe, Y. Harada, C. E. Sedwick, and J. Miller. 2004. Cutting edge: CD28-mediated transcriptional and posttranscriptional regulation of IL-2 expression are controlled through different signaling pathways. *J. Immunol.* 173: 7120–7124.
12. Tseng, S. Y., M. Liu, and M. L. Dustin. 2005. CD80 cytoplasmic domain controls localization of CD28, CTLA-4, and protein kinase Cθ in the immunological synapse. *J. Immunol.* 175: 7829–7836.
13. Varma, R., G. Campi, T. Yokosuka, T. Saito, and M. L. Dustin. 2006. T cell receptor-proximal signals are sustained in peripheral microclusters and terminated in the central supramolecular activation cluster. *Immunity* 25: 117–127.
14. Freiberg, B. A., H. Kupfer, W. Maslanik, J. Delli, J. Kappler, D. M. Zaller, and A. Kupfer. 2002. Staging and resetting T cell activation in SMACs. *Nat. Immunol.* 3: 911–917.
15. Sims, T. N., T. J. Soos, H. S. Xenias, B. Dubin-Thaler, J. M. Hofman, J. C. Waite, T. O. Cameron, V. K. Thomas, R. Varma, C. H. Wiggins, et al. 2007. Opposing effects of PKCθ and WASp on symmetry breaking and relocation of the immunological synapse. *Cell* 129: 773–785.
16. Benvenuti, F., C. Lagaudriere-Gesbert, I. Grandjean, C. Jancic, C. Hivroz, A. Trautmann, O. Lantz, and S. Amigorena. 2004. Dendritic cell maturation controls adhesion, synapse formation, and the duration of the interactions with naive T lymphocytes. *J. Immunol.* 172: 292–301.
17. Brossard, C., V. Feuillet, A. Schmitt, C. Randriamampita, M. Romao, G. Raposo, and A. Trautmann. 2005. Multifocal structure of the T cell - dendritic cell synapse. *Eur. J. Immunol.* 35: 1741–1753.
18. Campi, G., R. Varma, and M. L. Dustin. 2005. Actin and agonist MHC-peptide complex-dependent T cell receptor microclusters as scaffolds for signaling. *J. Exp. Med.* 202: 1031–1036.
19. Yokosuka, T., K. Sakata-Sogawa, W. Kobayashi, M. Hiroshima, A. Hashimoto-Tane, M. Tokunaga, M. L. Dustin, and T. Saito. 2005. Newly generated T cell receptor microclusters initiate and sustain T cell activation by recruitment of Zap70 and SLP-76. *Nat. Immunol.*
20. Wulfing, C., C. Sumen, M. D. Sjaastad, L. C. Wu, M. L. Dustin, and M. M. Davis. 2002. Costimulation and endogenous MHC ligands contribute to T cell recognition. *Nat. Immunol.* 3: 42–47.
21. Bromley, S. K., A. Iaboni, S. J. Davis, A. Whitty, J. M. Green, A. S. Shaw, A. Weiss, and M. L. Dustin. 2001. The immunological synapse and CD28-CD80 interactions. *Nat. Immunol.* 2: 1159–1166.
22. Egen, J. G., and J. P. Allison. 2002. Cytotoxic T lymphocyte antigen-4 accumulation in the immunological synapse is regulated by TCR signal strength. *Immunity* 16: 23–35.
23. Andres, P. G., K. C. Howland, D. Dresnek, S. Edmondson, A. K. Abbas, and M. F. Krummel. 2004. CD28 signals in the immature immunological synapse. *J. Immunol.* 172: 5880–5886.
24. Sparwasser, T., S. Gong, J. Y. Li, and G. Eberl. 2004. General method for the modification of different BAC types and the rapid generation of BAC transgenic mice. *Genesis* 38: 39–50.
25. Manders, E. M., J. Stap, G. J. Brakenhoff, R. van Driel, and J. A. Aten. 1992. Dynamics of three-dimensional replication patterns during the S-phase, analysed by double labelling of DNA and confocal microscopy. *J. Cell Sci.* 103: 857–862.
26. Borriello, F., M. P. Sethna, S. D. Boyd, A. N. Schweitzer, E. A. Tivol, D. Jacoby, T. B. Strom, E. M. Simpson, G. J. Freeman, and A. H. Sharpe. 1997. B7-1 and B7-2 have overlapping, critical roles in immunoglobulin class switching and germinal center formation. *Immunity* 6: 303–313.
27. Salomon, B., D. J. Lenschow, L. Rhee, N. Ashourian, B. Singh, A. Sharpe, and J. A. Bluestone. 2000. B7/CD28 costimulation is essential for the homeostasis of the $CD4^+CD25^+$ immunoregulatory T cells that control autoimmune diabetes. *Immunity* 12: 431–440.
28. Liang, S., P. Alard, Y. Zhao, S. Parnell, S. L. Clark, and M. M. Kosiewicz. 2005. Conversion of $CD4^+CD25^-$ cells into $CD4^+CD25^+$ regulatory T cells in vivo requires B7 costimulation, but not the thymus. *J. Exp. Med.* 201: 127–137.
29. Valitutti, S., M. Dessing, K. Aktories, H. Gallati, and A. Lanzavecchia. 1995. Sustained signaling leading to T cell activation results from prolonged T cell receptor occupancy: role of T cell actin cytoskeleton. *J. Exp. Med.* 181: 577–584.
30. Huppa, J. B., M. Gleimer, C. Sumen, and M. M. Davis. 2003. Continuous T cell receptor signaling required for synapse maintenance and full effector potential. *Nat. Immunol.* 4: 749–755.
31. Doty, R. T., and E. A. Clark. 1996. Subcellular localization of CD80 receptors is dependent on an intact cytoplasmic tail and is required for CD28-dependent T cell costimulation. *J. Immunol.* 157: 3270–3279.
32. Yokosuka, T., W. Kobayashi, K. Sakata-Sogawa, A. Hashimoto-Tane, M. L. Dustin, M. Tokunaga, and T. Saito. 2008. Spatiotemporal regulation of T cell co-stimulation by TCR-CD28 microclusters through PKC-θ translocation. *Immunity*, *In press*.
33. Heintz, N. 2001. BAC to the future: the use of bac transgenic mice for neuroscience research. *Nat. Rev. Neurosci.* 2: 861–870.
34. Shorter, J., and G. Warren. 2002. Golgi architecture and inheritance. *Annu. Rev. Cell Dev. Biol.* 18: 379–420.
35. Turley, S. J., K. Inaba, W. S. Garrett, M. Ebersold, J. Unternaehrer, R. M. Steinman, and I. Mellman. 2000. Transport of peptide-MHC class II complexes in developing dendritic cells. *Science* 288: 522–527.
36. Shen, S., Y. Ding, C. E. Tadokoro, D. Olivares-Villagomez, M. Camps-Ramirez, M. A. Curotto de Lafaille, and J. J. Lafaille. 2005. Control of homeostatic proliferation by regulatory T cells. *J. Clin. Invest.* 115: 3517–3526.
37. Bachmann, M. F., K. McKall-Faienza, R. Schmits, D. Bouchard, J. Beach, D. E. Speiser, T. W. Mak, and P. S. Ohashi. 1997. Distinct roles for LFA-1 and CD28 during activation of naive T cells: adhesion versus costimulation. *Immunity* 7: 549–557.
38. Wulfing, C., A. Bauch, G. R. Crabtree, and M. M. Davis. 2000. The vav exchange factor is an essential regulator in actin-dependent receptor translocation to the lymphocyte-antigen-presenting cell interface. *Proc. Natl. Acad. Sci. USA* 97: 10150–10155.
39. Al-Alwan, M. M., G. Rowden, T. D. Lee, and K. A. West. 2001. The dendritic cell cytoskeleton is critical for the formation of the immunological synapse. *J. Immunol.* 166: 1452–1456.
40. Benvenuti, F., S. Hugues, M. Walmsley, S. Ruf, L. Fetler, M. Popoff, V. L. Tybulewicz, and S. Amigorena. 2004. Requirement of Rac1 and Rac2 expression by mature dendritic cells for T cell priming. *Science* 305: 1150–1153.
41. Eun, S. Y., B. P. O'Connor, A. W. Wong, H. W. van Deventer, D. J. Taxman, W. Reed, P. Li, J. S. Blum, K. P. McKinnon, and J. P. Ting. 2006. Cutting edge: rho activation and actin polarization are dependent on plexin-A1 in dendritic cells. *J. Immunol.* 177: 4271–4275.
42. Itano, A. A., S. J. McSorley, R. L. Reinhardt, B. D. Ehst, E. Ingulli, A. Y. Rudensky, and M. K. Jenkins. 2003. Distinct dendritic cell populations sequentially present antigen to CD4 T cells and stimulate different aspects of cell-mediated immunity. *Immunity* 19: 47–57.
43. Bromley, S. K., and M. L. Dustin. 2002. Stimulation of naive T-cell adhesion and immunological synapse formation by chemokine-dependent and -independent mechanisms. *Immunology* 106: 289–298.
44. Dustin, M. L., and T. A. Springer. 1989. T-cell receptor cross-linking transiently stimulates adhesiveness through LFA-1. *Nature* 341: 619–624.
45. Jakus, Z., S. Fodor, C. L. Abram, C. A. Lowell, and A. Mocsai. 2007. Immunoreceptor-like signaling by β_2 and β_3 integrins. *Trends Cell Biol.* 17: 493–501.
46. Bates, M., B. Huang, G. T. Dempsey, and X. Zhuang. 2007. Multicolor super-resolution imaging with photo-switchable fluorescent probes. *Science* 317: 1749–1753.
47. Shen, K., V. K. Thomas, M. L. Dustin, and L. C. Kam. 2008. Micropatterning of costimulatory ligands enhances $CD4^+$ T cell function. *Proc. Natl. Acad. Sci. USA* 105: 7791–7796.